




## Article

# Anionic Azo Dyes: Wastewater Pollutants as Functionalizing Agents for Porous Polycarbonate Membranes Aiding in Water Decolorization

Alan Jarrett Messinger <sup>1</sup> , Isabella S. Mays <sup>2</sup> , Brennon Craigo <sup>1</sup>, Jeffrey Joering <sup>3</sup> and Sean P. McBride <sup>1,\*</sup> 

<sup>1</sup> Department of Mathematics and Physics, Marshall University, Huntington, WV 25755, USA; messinger29@marshall.edu (A.J.M.); craigo19@marshall.edu (B.C.)

<sup>2</sup> Biology Department, William & Mary, Williamsburg, VA 23186, USA; ismays@wm.edu

<sup>3</sup> Department of Physics, Geology & Engineering Technology, Northern Kentucky University, Highland Heights, KY 41099, USA; joeringj2@mymail.nku.edu

\* Correspondence: mcbrides@marshall.edu

## Abstract

Efficient water decolorization techniques are vital for ensuring fresh water for future generations. Azo dyes are used heavily in the textile industry and are a challenge to remove from industrial wastewater. This research expands on recent innovative work where anionic azo dyes themselves were used to functionalize track-etched porous polycarbonate filtration membranes with decolorized water obtained as a byproduct. The objective of this research is to determine whether the observed dye rejection is dependent on the magnitude of the intrinsic charge of the dye molecule or on its structure, using two selectively chosen anionic azo dye series during functionalization. The first group is a negative two intrinsic charge series with six dyes, each differing in structure, and the second group is a five-dye series that increases from  $-1$  to  $-6$  in intrinsic charge. Rejection measurements as a function of both time and concentration during functionalization are made using ultraviolet-visible light spectroscopy. For  $100\ \mu\text{M}$  aqueous dyes, comparing pre- and post-functionalization, a systematically increasing trend in the ability to functionalize porous polycarbonate based on the number of double 6-carbon ring structures in the dyes is illustrated and found to be independent of intrinsic charge.

**Keywords:** rejection; membranes; filtration; water; pollution; chemical structure; charge; purification; textiles



Academic Editors: Cristina-Gabriela Grigoraş and Andrei Ionut Simion

Received: 28 July 2025

Revised: 16 August 2025

Accepted: 22 August 2025

Published: 26 August 2025

**Citation:** Messinger, A.J.; Mays, I.S.; Craigo, B.; Joering, J.; McBride, S.P.

Anionic Azo Dyes: Wastewater Pollutants as Functionalizing Agents for Porous Polycarbonate Membranes Aiding in Water Decolorization. *Sustainability* **2025**, *17*, 7696. <https://doi.org/10.3390/su17177696>

**Copyright:** © 2025 by the authors. Licensee MDPI, Basel, Switzerland. This article is an open access article distributed under the terms and conditions of the Creative Commons Attribution (CC BY) license (<https://creativecommons.org/licenses/by/4.0/>).

## 1. Introduction

On geological time scales, the  $1.4 \times 10^{18}\ \text{m}^3$  of water that is constantly being transferred between Earth's oceans, atmosphere, and landscape, forming a closed cycle, will not diminish [1,2]. However, despite this large volume of water contained in Earth's water cycle, only 2.5% of all water on Earth is fresh water, with only 0.3% being accessible in freshwater lakes and rivers [3]. History has dictated that access to safe water is the seed for thriving civilizations [4,5]. With the growth of modern civilizations comes industrial revolutions, with some industries expelling toxic substances that end up in the atmosphere, soil, oceans, lakes, and rivers [6]. The world population continues to grow, with the present count being over 8.2 billion people [7,8]. The combination of a growing population in modern industrialized civilizations and limited safe water resources has created regions on Earth with ever-increasing water scarcity [9].

The modern textile industry is one of the largest users of available fresh water, second to the agricultural industry, and is responsible for 4% of the fresh water consumed per year [10]. Dyes in the textile industry are used in the production of everyday items, such as papers, inks, soaps, detergents, cosmetics, pharmaceuticals, lacquers, plastics, and leather products, among others [11,12]. Annually, 80 billion new clothing items are purchased that are made through the various steps of production (washing, bleaching, dyeing, etc.) via the textile industry, an industry that results in approximately 20% of the world's wastewater [10,13]. The fashion industry is the second biggest polluter in the world, just behind the oil and gas industry [10]. It is estimated that roughly  $2.8 \times 10^5$  tons of textile dyes are discharged into the environment each year, creating negative effects on human health and the surrounding ecosystem [14,15]. Only 0.8% of the Earth's surface is composed of freshwater habitats, yet they remain threatened by human pressures—including pollution—leading to a decrease in overall habitat biodiversity [16]. For example, aquatic vegetation is extremely important in keeping freshwater habitats in a desired low turbidity state. Aquatic vegetation is sensitive to the underwater light environment and can decline in poor water quality and deteriorated light environments [17]. Concentrations of  $1 \text{ mg}\cdot\text{L}^{-1}$  for some dyes can be visible in aquatic environments, which could lead to altering the quality of the water for aquatic vegetation [18]. It has been shown that the amount of light present underwater, and thus clarity of water, tends to be enhanced by aquatic vegetation, creating a positive feedback loop in a clear-water vegetation-dominated state [19].

The global textile industry is seemingly an unmovable fixture of our modern society [20]. Many recent innovative methods have been demonstrated to aid in removing dye pollutants from water, such as using biosynthesized nickel oxide nanoparticles [21], biosynthesis of zero-valent iron graphene nanocomposites [22], the Fenton oxidation process at varying pH levels [23], adsorption via absorbents that are alternatives to costly activated carbon [24], polysulfide/polyetherimide ultrafiltration composite membranes [25,26], and immobilized algae with biodegradation [27], among many other recent innovative methods [28]. These recent methods are not meant to be an exhaustive list of all recent methods, but rather a diverse collection of experiments. They illustrate that when investigating removal or decolorization methods, typically one or a small group of dyes is used [22,23,28], while few experiments use dye groups containing at least six dyes [21].

Azo dyes are prevalent, making up approximately 60% of all dyes and 70% of all dyes used in industry [29]. Azo dyes are dyes that have the presence of at least one diazenyl functional group ( $-\text{N}=\text{N}-$ ), or azo group, joining two aryl or alkyl groups of varying compositions [29,30]. A subtype of azo dyes is direct (or substantive) azo dyes. Any anionic water-soluble dye that has a strong affinity for cellulose fibers when applied after being added to water containing an electrolyte is a direct dye [31]. One advantage of the decolorization method used in this work is that the azo bond is not broken, preventing the creation of possible dangerous aromatic amines.

Previous research has shown that (1) when specific anionic direct azo dyes were filtered through a porous polycarbonate membrane at relatively high concentrations ( $1000 \mu\text{M}$ ), the flow rate of the dye decreases while the percent rejection of the dye molecules themselves increases and (2) an increase in percent rejection of low concentration dyes was present after high concentrations of dyes ( $50\text{--}1000 \mu\text{M}$ ) were already pulled through the porous polycarbonate membranes to first functionalize them [32]. The research presented here aims to determine whether the observed increase in rejection between pre- and post-functionalization is heavily dependent on the magnitude of the dye molecule's intrinsic charge in its chemical structure by using 10 dyes with varying intrinsic charges and structures. Here, intrinsic charge is defined as the number of charge sites left on the dye molecule associated with the functional groups ( $\text{SO}_3^{3-}$ ) and carboxylate functional groups ( $\text{COO}^-$ )

after the dye goes through dissociation in type 1 water. Additionally, the word ‘functionalize’ (and variations of it) is used to describe the summative interactions between the dye molecule and the polycarbonate filter that are responsible for the observed effects. Quantitative measurements are needed to determine the exact mechanisms responsible for the observed effects. To test the intrinsic charge dependency, both the physical structure and functional end groups were kept the same as often as possible; thus, all dyes used were direct anionic azo dyes.

Gaining an understanding of the variables that influence the functionalization process and increase dye rejection can, in turn, be used to optimize such membrane functionalization for future water decoloring processes and technologies. Generally, it is accepted that dye molecules used in the textile industry interact with the fibers to be dyed via ionic interactions, Van der Waals forces, hydrogen interactions, and covalent bonds depending on the substrate and dye; however, not much information is available on how direct anionic azo dyes interact with polycarbonate membranes [33–35].

## 2. Materials and Methods

### 2.1. Dyes

Two selectively chosen dye series were tested as functionalizing agents for commercially available porous polycarbonate filters. The first criterion for the dyes chosen was that they all belong to the same chemical family, thus, anionic direct azo dyes. Azo dyes were selected because they are used heavily in the textile industry. The second characteristic was that they had to have either the same charge but varying structure or a systematically different charge independent of structure. The third characteristic was that the dyes had to be readily available from manufacturers, requiring no specialized synthesis. The fourth characteristic was that they had to be cost-effective to purchase, providing enough material for testing for current and future experiments.

For the negative two intrinsic charge series, the following dyes were used: direct red 28 ([DR 28, congo red], Thermo Scientific, Waltham, MA, USA), direct red 81 ([DR 81, chlorantine fast red 5B], Tokyo Chemical Industry Co., Ltd., Nihonbashi-honcho, Chuo-ku, Tokyo, Japan), direct brown 2 ([DBW 2, direct fast brown M], Tokyo Chemical Industry Co., Ltd., Nihonbashi-honcho, Chuo-ku, Tokyo, Japan), direct red 2 ([DR 2, benzopurpurin 4B], Thermo Scientific, Waltham, MA, USA), direct red 37 ([DR 37], Tokyo Chemical Industry Co., Ltd., Nihonbashi-honcho, Chuo-ku, Tokyo, Japan), and direct yellow 12 ([DY 12, chrysophenine], Tokyo Chemical Industry Co., Ltd., Nihonbashi-honcho, Chuo-ku, Tokyo, Japan); their chemical structures are shown in Figure S1 (images obtained from the PubChem database [36–41]). For the increasing intrinsic charge series, the following dyes were used: direct yellow 8 ([DY 8], Tokyo Chemical Industry Co., Ltd., Nihonbashi-honcho, Chuo-ku, Tokyo, Japan), direct red 28, direct blue 2 ([DB 2], Tokyo Chemical Industry Co., Ltd., Nihonbashi-honcho, Chuo-ku, Tokyo, Japan), direct blue 14 ([DB 14], Tokyo Chemical Industry Co., Ltd., Nihonbashi-honcho, Chuo-ku, Tokyo, Japan), and direct yellow 106 ([DY 106, Permalite Yellow EFC 200%], Standard Colors, Inc., High Point, NC, USA); their chemical structures are shown in Figure S2 (images obtained from PubChem [36,42–45]). The series increases from  $-1$  to  $-4$  and ends with a  $-6$  intrinsic charge. A dye with a  $-5$  intrinsic charge was desired for the intrinsic charge series but was not obtained. All dyes were used as received.

Overall, for each dye, six aqueous solutions with type 1 water were made following the systematically increasing concentrations of 50  $\mu\text{M}$ , 100  $\mu\text{M}$ , 250  $\mu\text{M}$ , 500  $\mu\text{M}$ , 750  $\mu\text{M}$ , and 1000  $\mu\text{M}$ . A 575 mL solution of the 1000  $\mu\text{M}$  is made first, saving aliquots of 25 mL and 50 mL samples to make 500 mL volumes of 50  $\mu\text{M}$  and 100  $\mu\text{M}$  solutions via dilution. All other concentrations are made independently with no dilutions. Additional fine details

of the dye solution preparation method can be found in Section S1 of the Supplemental Material File. All dyes were made fresh and used immediately for experiments. All tests relating to functionalization of the polycarbonate membranes in this work were performed at room temperature and at the native pH of the solutions at their respective concentrations without the addition of any mordant.

## 2.2. Sample Collection

Information found in previous work, such as (i) detailed images and fine fabrication details used to create the custom 500 mL capacity glass filtration chambers shown in Figure 1, (ii) details describing the modification of polypropylene filter holders used in this work, and (iii) atomic force and electron scanning microscopy images of the bare porous polycarbonate filters used in this experiment, need not be duplicated in great detail here. A brief overview of the operation in this section and Section 2.3 is provided for clarity [32]. One addition in this work is that three identical filtration chambers with identical performances were used to collect data, with the primary difference between the setups being the brand of tunable vacuum pump used.

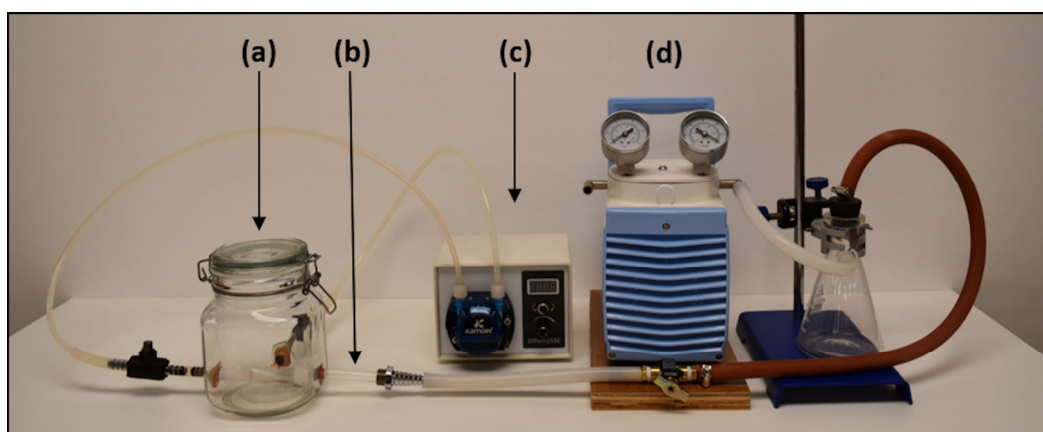


**Figure 1.** A complete setup for sample collection showing (a) a custom-fabricated filtration chamber, (b) the syringe collection vessel, (c) the peristaltic pump, and (d) the tunable vacuum pump. A detailed schematic of the custom-fabricated filtration chamber is also available [32] (Figure 4).

The following provides a brief description of the setup and sample collection protocol using the custom filtration chambers labeled as (a) in Figure 1. Prior to any direct dye tests, the custom-fabricated filtration chambers were rigorously cleaned with a 1% by mass aqueous Alconox solution (Alconox, Inc., White Plains, NY, USA) followed by copious rinsing with tap water and then a rinse with copious amounts of type 1 water (Direct Q3-UV, MilliporeSigma, St. Louis, MO, USA). After a similar Alconox washing and rinsing with tap water, the modified polypropylene filter holders (Swinnex Filter Holder, MilliporeSigma, St. Louis, MO, MA, USA) and stainless-steel photoetched support screens (MilliporeSigma, St. Louis, MO, USA) used to support the polycarbonate filters both received an additional 5–20 min sonication in 50 °C aqueous Elma Tec Clean A4 solution (Elma Schmidbauer GmbH, Singen, Baden-Württemberg, Germany) at a pH  $\approx$  10–11 and were then rinsed with copious amounts of tap water prior to a final rinse with copious amounts of type 1 water. Similarly, all glassware used in the experiments for short-term dye solution storage was cleaned in a similar manner following this Alconox wash, tap water rinse, heated sonicator cleaner wash, tap water rinse, and then type 1 water rinse procedure, with glassware finally being dried in a gravity oven (100 L gravity convection oven, Thermo Scientific, Waltham, MA, USA). Silicone gaskets (MilliporeSigma, St. Louis, MO, USA), specifically designed for the 13 mm Swinnex filter holders, are used to compress the polycarbonate filter and

steel support screen together in the modified polypropylene housing. O-rings (Danco, Inc., Irving, TX, USA) of various sizes were added to the modified polypropylene assembly containing the polycarbonate filter, steel support screen, and silicone gaskets, which helped make a leak-proof seal, as the assembly is threaded into the custom filtration chamber wall. With all intake and outflow circulation valves closed (or alternatively open with proper tubing connected, as shown in Figure 1), the desired solution, either water or a 500 mL dye solution, is then poured into the filtration chamber for use. At the completion of a dye test, the dye is transferred out of the filtration chamber. The chamber and all components are rinsed thoroughly with type 1 water until no color is seen in the wastewater, which is stored for removal.

To remove any large-scale concentration gradients in solution or buildup of rejected dye molecules at the filter surface during filtration, a peristaltic pump, labeled (c) in Figure 1 (DIPump550, Kamoer Fluid Tech (Shanghai) Co., Ltd., Shanghai, China), operating at  $\sim 108 \mu\text{L}\cdot\text{min}^{-1}$  is used to circulate the dye solutions through the system and to ensure a direct, continuous, high-speed flow of fluid over the surface of the porous polycarbonate filter. The peristaltic pump is on only when fluid is being pulled through the filter. Hydrophilic track-etched polycarbonate filters, 13 mm in diameter, with 100 nm-diameter pores (Isopore Membrane Filters, Millipore Sigma, St. Louis, MO, USA), were used as received from the manufacturer. The pressure differential that pulls the dye solutions through the polycarbonate filter, thus functionalizing the filter, is provided by vacuum pumps, labeled (d) in Figure 1, operating at a constant tunable pressure of 77.9 kPa/23 inHg for all experiments in this study (Models: GM-0.50, Huanyu, Hangzhou, China; 0.5A, Choicest Equip, Chengdu City, China; WP6111560, Millipore, Burlington, MA, USA). Before entering the vacuum line trap, the permeate is collected safely in a collection chamber consisting of a standard syringe vessel, labeled (b) in Figure 1. The male Luer slip inlet of the syringe vessel fits tightly into the modified filter housings' female Luer lock outlet that is threaded into the filtration chamber wall.

Any changes in variables such as pressure, pore size or porosity of the polycarbonate filter, type of filter, type of dye, and concentration of dye would cause a change in the flow rate. By keeping these variables as constant as possible, the variables that affect the functionalization of the porous polycarbonate filter can be narrowed.

### 2.3. Rejection and Flow Rate Measurements

Feed samples and permeate samples were taken at specified intervals and analyzed via ultraviolet-visible light spectroscopy (ND-1000 Spectrophotometer, NanoDrop Technologies, Inc., Wilmington, DE, USA), which was used to measure the absorbance and thus the concentrations of the samples. The absorbance was linearly dependent on the concentration for the dyes tested due to a molecule's energy absorption properties; thus, the concentration was determined from the absorbance [46]. For absorbance measurements, a path length of 1.0 mm was used as much as possible for less optically dense dyes, typically at 500  $\mu\text{M}$  or below, while more optically dense dyes at higher concentrations typically required a path length of 0.2 mm to obtain meaningful data. Knowing the concentrations of the dyes in solutions allows for the calculation of the rejection of the dye molecules through Equation (1). In Equation (1),  $R$  is the rejection in percent, while  $C_P$  and  $C_F$  are the concentrations in the permeate and the feed, respectively.

$$R = \left(1 - \frac{C_P}{C_F}\right) \times 100 \% \quad (1)$$



The absorption of each sample was measured three times and averaged to ensure confidence in the measurements. The amount of fluid used for these spectroscopic measurements ranged from 2.0 to 2.5  $\mu\text{L}$ .

Permeate samples are massed using a precision balance (OHAUS PX224 Pioneer Analytical Balance with 0.0001 g resolution, Parsippany-Troy Hills, NJ, USA), and the density of water is used to calculate the volume of the permeate in  $\mu\text{L}$ . The volume, combined with the specified time of data collection, easily allows for the determination of the flow rate in  $\mu\text{L}\cdot\text{min}^{-1}$ . Only small aliquots of test fluid on the order of several hundred  $\mu\text{L}$  to 1 mL were pulled through the filter at various times as the permeate, leading to the 500 mL of test fluid in the custom filtration chamber being considered an infinite reservoir of constant concentration feed solution.

#### 2.4. Two-Hour Tests

Two-hour tests are performed for each dye at 1000  $\mu\text{M}$  to see how each dye functionalizes the polycarbonate membranes as a function of time. In these tests, the total time the dye is being pulled through the filter is 2 h, which allows most dyes to reach a stable rejection value with only minor deviations not exceeding 1.1% in the last 30 min of test time. As results show, most of the functionalization occurs in the first 15–20 min of dye test time. A combination of one-, two-, four-, five-, or six-minute tests is used to capture the functionalization process over 2 h. Typically, 11 one-minute tests are conducted first, followed by 3 two-minute tests, then times are adjusted as needed. Only 2-h tests where the flow rates decreased nearly monotonically as a function of time and the rejection increased nearly monotonically as a function of time were considered valid tests; any tests with excessive jumps in flow rate or rejection were not considered valid and excluded from the study. All 2-h tests presented are for single runs, resulting in no error bars on flow rate plots. The error bars on rejection plots for 2-h tests are the standard deviation of three measurements on the same sample, with error bars typically being smaller than the data points.

#### 2.5. Hysteresis Tests

Hysteresis tests are performed for each dye to see how each dye functionalizes the polycarbonate membranes as a function of concentration. During these tests, 15 min of dye at each concentration is pulled through the filter using 5 three-minute tests, with the last 4 of those measurements analyzed for reporting; the first data point in the 5 data point series is excluded, as this first flush is observed to wash out the previous test fluid. Between dye concentrations in these hysteresis tests, 15 min of type 1 water is flushed through the filters in 3 five-minute tests to remove any unbound dye molecules at each concentration during functionalization. The concentrations of the dye are first tested at 50  $\mu\text{M}$  and increased systematically at the pre-made concentrations up to 1000  $\mu\text{M}$ , and then back down from 1000  $\mu\text{M}$  to 50  $\mu\text{M}$  at the same concentrations. Hysteresis tests performed in this manner help to exemplify any functionalization of the polycarbonate filter by the dyes. If the dye molecules were not functionalizing the filter, there would be no change in rejection or flow rate values as the dye concentration is increased and then decreased again back to the starting concentration. Or, alternatively, any hysteresis in flow rate or rejection as concentration is decreased, after already being increased, can be attributed to dyes functionalizing the polycarbonate membrane at higher concentrations. Error bars on graphs of this type in the data file represent the standard deviation in the last four of the five 3-min tests at each dye concentration. All hysteresis tests presented are for single runs.

### 3. Results and Discussion

All dye solution absorbances were tested as a function of concentration, ensuring all were well-defined, linear relationships as expected. Figure S3 illustrates the high degree of precision of the solutions made for these experiments using the technique outlined in Sections 2.1 and 2.3. Dye samples were either measured prior to first use in the filtration chamber or measured from samples in situ during the hysteresis tests in the filtration chambers. The largest r-squared value that deviated from 1.0 was 0.9991, and the largest offset from an expected zero intercept was 0.0059 a.u., both values indicating the solutions were made with a high degree of precision.

For both the 2-h tests and hysteresis tests, new non-functionalized polycarbonate filters are first flushed with type 1 water over a 15-min interval (five 3-min measurements). This first flushing with clean water should produce a constant flow rate. This step helps ensure no fouling is present in the filters, and thus the filtration chambers are clean. This flushing also helps to characterize the filters prior to dye functionalization. A similar minimum 15-min type 1 water flush is performed post-functionalization to see how much the functionalization has altered the type 1 water flow rate. As shown in Table 1, all polycarbonate filters have stable initial water flow rates based on the low standard deviation (five 3-min measurements), indicating no fouling, but have a wide distribution of initial water flow rate values. Variations in initial type 1 water flow rates exceeding  $100 \mu\text{L}\cdot\text{min}^{-1}$  related to using different polycarbonate membranes with different stainless steel support screens are documented in the Supplemental Material File, Section S2.

When collecting data during the 2-h tests, it is observed that most dyes have drastically different ending values for final dye rejection and final dye flow rate. The same observation is present when examining the hysteresis tests, where the highest concentration of dye is used. All these factors in combination create challenges for direct data comparisons between the dyes. To investigate similarities and trends in visual rates of functionalization, dye rejection, and flow rate data, simple equations were developed to normalize the data, allowing for effective visual comparison of the data sets. Dyes with similar performance characteristics for functionalizing the polycarbonate filters should collapse into a single family of curves after such a normalization. The flow rate and rejection data for direct red 28 and direct red 2 are used as examples for the development of these normalization equations. Normalizing, or zeroing, the rejection hysteresis data is described below. Similar details of zeroing hysteresis flow rate data and data obtained during the 2-h tests are provided in the Supplemental Material File, Section S3.

In Equation (2),  $R_Z$  is the zeroed rejection value, and  $R$  is the recorded rejection value at a specified concentration.  $R_I$  refers to the 1000  $\mu\text{M}$  rejection increasing concentration data point value, while  $R_D$  refers to the 1000  $\mu\text{M}$  rejection decreasing concentration data point value at 1000  $\mu\text{M}$ . Figure 2 illustrates the use of Equation (2) in zeroing the hysteresis rejection data for direct red 2.

$$R_Z = R - \left( \frac{R_I + R_D}{2} \right) \quad (2)$$

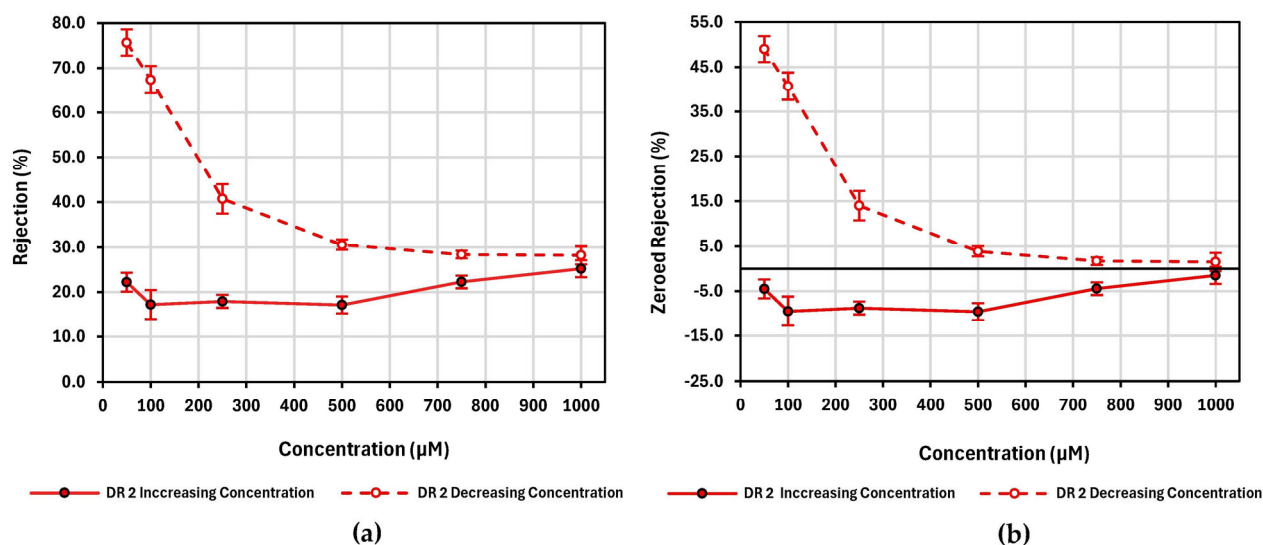
Figures 2 and S6–S8 show that the shapes of the rejection and flow rate graphs are unaltered during these zeroing processes but are merely shifted on their vertical axis, placing emphasis on the data at the end of the test, where data will align. For rejection as a function of time tests, zeroing the data helps visualize trends that can be seen while the dye is functionalizing the filter at a high constant concentration of 1000  $\mu\text{M}$  for 120 min. For hysteresis tests, the zeroing method used specifically helps visualize the change (hysteresis) between the beginning and ending data points at the 100  $\mu\text{M}$  concentrations as the concentration is increased and then decreased.

**Table 1.** Pre- and post-experimental flow rates of type 1 water through polycarbonate filters used in this study over 15-min intervals. Pre-H<sub>2</sub>O values correspond to the 15 min prior to the dye being studied, and the post-H<sub>2</sub>O values correspond to the last 15 min of the wash cycle after a dye test is complete.

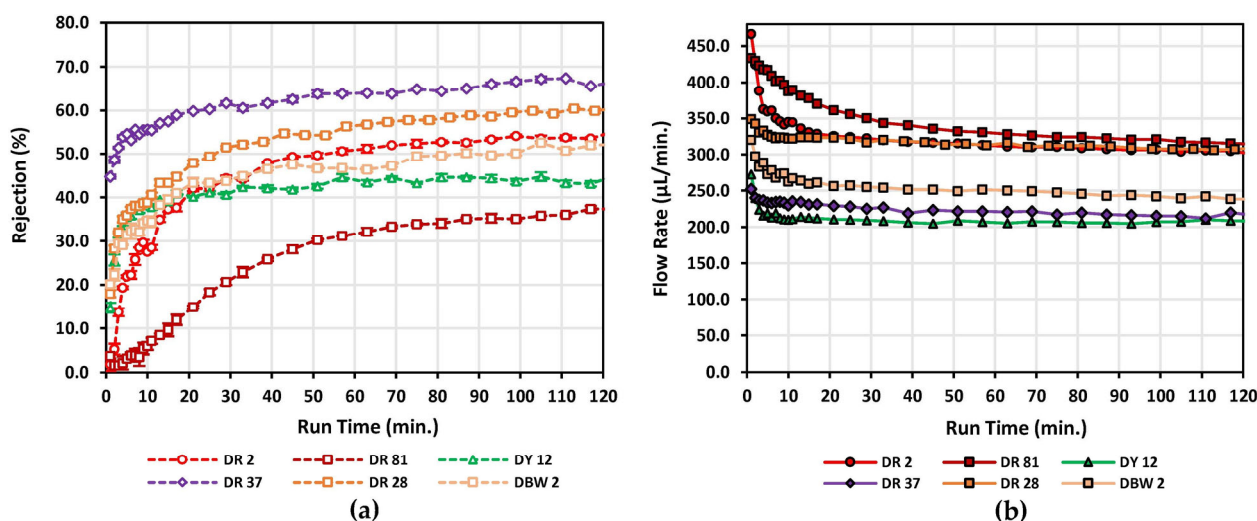
		Pre-H <sub>2</sub> O Flow Rate		Post-H <sub>2</sub> O Flow Rate		
Dye	Charge	$\left(\mu\text{L}\cdot\text{min}^{-1}\right)$		$\left(\mu\text{L}\cdot\text{min}^{-1}\right)$		% Decrease
		Ave	Std	Ave	Std	
2 h −2 Intrinsic Charge Series Pre- and Post-Water Flow Rates						
DR 2	−2	510.0	4.2	382.7	1.6	25.0
DR 81	−2	441.8	2.1	366.9	1.6	17.0
DBW 2	−2	377.7	0.4	324.4	3.0	14.1
DR 28	−2	390.2	2.3	367.2	2.6	5.9
DY 12	−2	347.0	2.9	338.9	2.9	2.3
DR 37	−2	341.9	1.9	337.4	1.7	1.3
2 h Increasing Charge Series Pre- and Post-Water Flow Rates						
DY 8	−1	484.5	4.3	426.4	3.5	12.0
DR 28	−2	390.2	2.3	367.2	2.6	5.9
DB 2	−3	375.7	0.7	325.0	1.4	13.5
DB 14	−4	360.1	4.0	348.8	2.7	3.1
DY 106	−6	352.8	1.8	244.8	2.7	30.6
Symmetric Sulphonate Series Hysteresis Pre- and Post-Water Flow Rates						
DR 2	−2	449.9	2.1	365.3	2.5	18.8
DR 28	−2	356.1	1.6	297.1	2.0	16.6
DB 2	−3	462.3	4.0	339.3	19.9	26.6
DB 14	−4	501.9	4.3	395.4	17.5	21.2
DY 106	−6	390.6	2.6	152.2	0.8	61.0
Asymmetric Sulphonate Series Hysteresis Pre- and Post-Water Flow Rates						
DY 8	−1	423.7	6.1	363.0	4.6	14.3
DBW 2	−2	488.4	3.2	296.7	4.8	39.3
DY 12	−2	485.6	2.5	406.7	0.9	16.2
DR 37	−2	523.2	2.4	447.6	45.4	14.5
DR 81	−2	383.2	2.7	349.5	1.9	8.8

Figure 3 illustrates the non-zeroed results of the 2-h tests for the six anionic azo dyes with an intrinsic charge of negative two at a concentration of 1000  $\mu\text{M}$ , each pulled through separate unmodified polycarbonate filters. All negative two azo dyes exhibited post-azo-dye-functionalization water flow rates that had decreases ranging from 1.3% for direct red 37 to 25.0% for direct red 2 during the last 15 min of post-wash cycles with type 1 water, where the water flow rate stabilized. All such post-azo-dye-functionalization type 1 water flow rates for all experiments are found in Table 1. If the water flow rates do not return to their initial water flow rate prior to any dye tests, then this indicates the modifications to the surface of the polycarbonate by the direct azo dyes are permanent within the experimental setup. It is important to note that if the water flow rate remains stable during the dye washout at the end of the test, no unbound dye is being removed. Likewise, if the dye flow rate remains stable during dye tests, the filter is no longer being functionalized; a slow, decreasing flow rate with gradually increasing rejection can be seen after approximately 30 min for most dyes in Figure 3.





**Figure 2.** (a) Raw direct red 2 (DR 2) rejection data as a function of concentration; (b) zeroed direct red 2 (DR 2) rejection data as a function of concentration.



**Figure 3.** (a) Non-zeroed rejection as a function of time for the  $-2$  intrinsic charge series at 1000  $\mu\text{M}$ ; (b) non-zeroed flow rate as a function of time for the  $-2$  intrinsic charge series at 1000  $\mu\text{M}$ . Closed data points represent flow rate values, and open data points represent rejection values. Red circles—direct red 2 (DR 2), dark red squares—direct red 81 (DR 81), green triangles—direct yellow 12 (DY 12), purple diamonds—direct red 37 (DR 37), orange squares—direct red 28 (DR 28), and light brown squares—direct brown 2 (DBW 2).

Figure 3 clearly demonstrates that while having the same intrinsic charge, these anionic azo dyes interact with the polycarbonate membrane differently. For the last sample post-functionalization during the 120-min test, rejection values ranged from  $37.4 \pm 0.7\%$  for direct red 81 to  $66.6 \pm 0.5\%$  for direct red 37, with dye flow rate values ranging from  $207.9 \mu\text{L}\cdot\text{min}^{-1}$  for direct yellow 12 to  $314.4 \mu\text{L}\cdot\text{min}^{-1}$  for direct red 81. Direct red 2 had the largest increase in rejection from beginning to end, starting at a rejection value of  $1.8 \pm 1.4\%$  and ending with a rejection value of  $55.3 \pm 0.7\%$  post-functionalization. Direct red 37 had the smallest difference in rejection from beginning to end, having a starting rejection value of  $44.7 \pm 0.4\%$  and an ending rejection value of  $66.6 \pm 0.5\%$ . This data is likely a result of not being able to capture the fast functionalization between time equals zero and the end of the first one-minute test; otherwise, direct red 37 would likely have the largest difference in rejection from beginning to end. Direct red 81, while having the lowest

rejection value of the negative two intrinsic charge series, still has a systematic increase in rejection with a systematic decrease in flow rate, though at a much different rate than that of the other dyes tested. Direct red 2 presented challenges in collecting due to its affinity for the polypropylene collection vessel; despite this, the flow rate as a function of time graph is nearly monotonically decreasing with few deviations. If intrinsic charge alone were the dominant factor during functionalization, all these dyes would have similar trends as a function of time and reach similar ending rejection values. All raw data for the entirety of this project is available in the publicly accessible data files, with access information for those files found at the end of this article.

Figure 4 illustrates the same end results of the two-hour tests in Figure 3, but zeroed. While each of these dyes shares the same negative two intrinsic charge, they differ heavily in rejection and flow rate trends after being zeroed, again demonstrating that intrinsic charge alone is not a dominant parameter in determining rejection and functionalization.

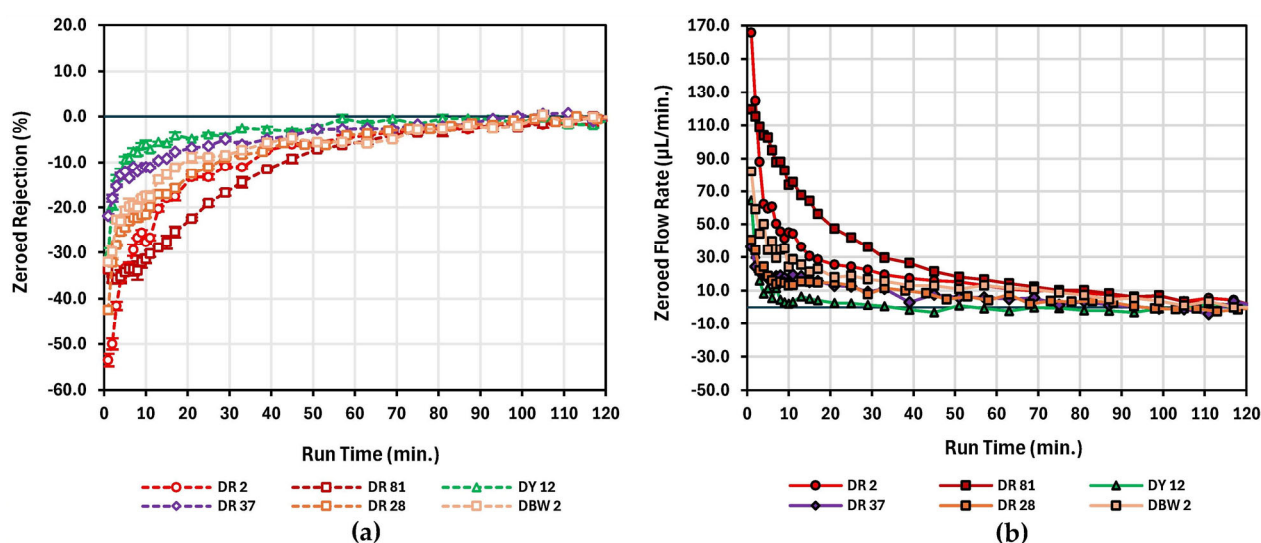


**Figure 4.** (a) Zeroed rejection as a function of time for the  $-2$  intrinsic charge series at  $1000\ \mu\text{M}$ ; (b) zeroed flow rate as a function of time for the  $-2$  intrinsic charge series at  $1000\ \mu\text{M}$ . Closed data points represent flow rate values, and open data points represent rejection values. Red circles—direct red 2 (DR 2), dark red squares—direct red 81 (DR 81), green triangles—direct yellow 12 (DY 12), purple diamonds—direct red 37 (DR 37), orange squares—direct red 28 (DR 28), and light brown squares—direct brown 2 (DBW 2).

Figure 5 illustrates the non-zeroed results of the 2-h tests for each of the five anionic azo dyes that increased in intrinsic charge from negative one to negative six at  $1000\ \mu\text{M}$ , each of which was pulled through separate unmodified polycarbonate filters. As shown in Table 1, all negatively charged azo dyes exhibited post-azo-dye-functionalization, as type 1 water flow rates had decreases in flow rate ranging from 3.1% for direct blue 14 to 30.6% for direct yellow 106 during the last 15 min of post-wash cycles with water, where the water flow rate stabilized. Such stable flow rates again indicate the functionalization is permanent under the conditions of the experiment. Ending dye flow rates ranged from  $189.8\ \mu\text{L}\cdot\text{min}^{-1}$  for direct yellow 106 to  $370.8\ \mu\text{L}\cdot\text{min}^{-1}$  for direct yellow 8. The outlier in Figure 5 appears to be direct yellow 8, based primarily on rejection as a function of time data. Direct yellow 8 differs in the shape of the rejection curve, which is also shifted towards lower rejection values. Direct yellow 8 rejects the least, with a rejection value of  $42.6\% \pm 0.3\%$  for the last sample taken post-functionalization. Direct blue 14 has the lowest increase in rejection, starting at a rejection value of  $20.0 \pm 2.8\%$  and ending at a rejection value of  $51.9 \pm 1.3\%$ . Direct yellow 106 has one of the highest final rejection values

of  $62.2 \pm 0.5\%$ , while having an intrinsic charge of negative six. This rejection value is close to the rejection value of  $60.4 \pm 0.3\%$  for direct red 28, an azo dye with an intrinsic charge of negative two, again indicating that intrinsic charge is not the dominant parameter dictating a dye's rejection capabilities with polycarbonate. Direct yellow 106 has the largest increase in rejection for this series, starting at a rejection value of  $14.2 \pm 1.0\%$  and ending at a rejection value of  $62.2 \pm 0.5\%$ . Almost all error bars for the tests per sample are smaller than the data points, with the exception being direct blue 14, which displays a standard deviation of a few percent in terms of rejection. Like direct red 2, direct blue 14 presented challenges for collecting due to its affinity for the polypropylene collection vessel; despite this, the flow rate as a function of time graph is nearly monotonically decreasing with few deviations. Including all dye results for this series, there appears to be no correlation of ending rejection values to intrinsic charge.

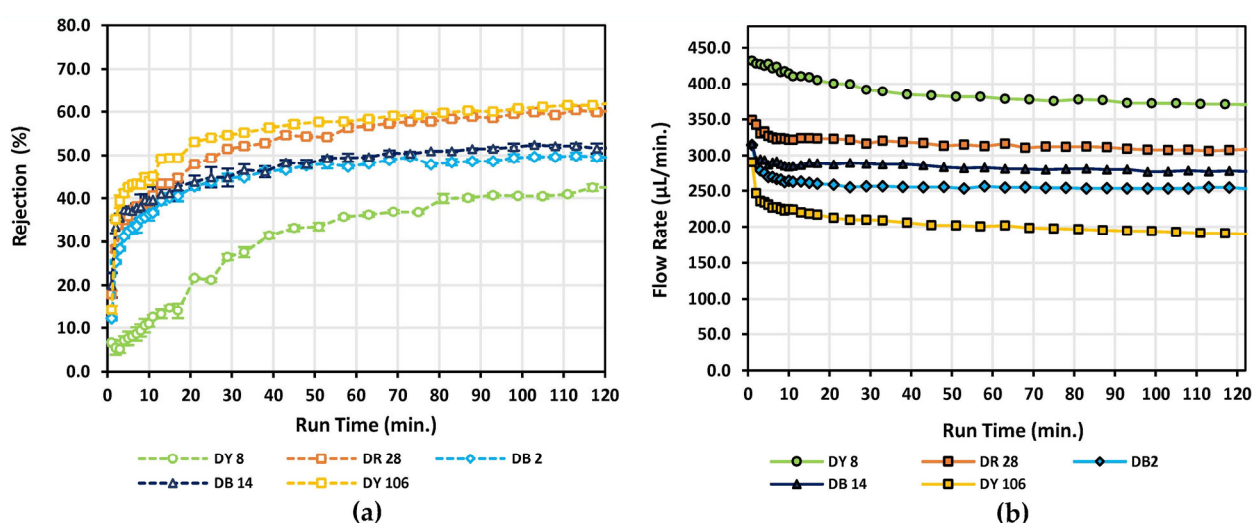


**Figure 5.** (a) Non-zeroed rejection as a function of time for the increasing intrinsic charge series at 1000  $\mu\text{M}$ ; (b) non-zeroed flow rate as a function of time for the increasing intrinsic charge series at 1000  $\mu\text{M}$ . Closed data points represent flow rate values, and open data points represent rejection values. Light green circles—direct yellow 8 (DY 8), orange squares—direct red 28 (DR 28), light blue diamonds—direct blue 2 (DB 2), dark blue triangles—direct blue 14 (DB 14), and yellow squares—direct yellow 106 (DY 106).

When examining Figures 3 and 5, one can hypothesize based on the data that the rejection values would, in theory, start at zero for each dye tested, but the one-minute tests in the experiment were simply not able to capture the fast dynamics at smaller time steps. Sample times of less than one minute are undesirable, given the limitations of the current system, where achieving an instant vacuum is not possible, and fractional uncertainties in the vacuum levels at the start of tests will increase if test times are shorter than one minute.

Figure 6 illustrates the same results of the two-hour tests for the increasing intrinsic charge series as in Figure 5, but zeroed. The changes in the rejection and flow rates seen for all dyes in the increasing intrinsic charge series indicate that these dyes are each interacting with the filters differently, with most creating modifications to the polycarbonate that are permanent, as shown in Table 1 based on type 1 water flow rates post-functionalization. Figure 6 also demonstrates that dye rejection and flow rates have no overarching correlation with the increase in intrinsic charge, though more correlation is present than the negative two intrinsic charge series data presented in Figure 4. All dyes in this series, besides direct yellow 8, independent of intrinsic charge, have similar structures for the end groups, which is the first indication that dye structure may play a more dominant role in the functionalization process compared to intrinsic charge.

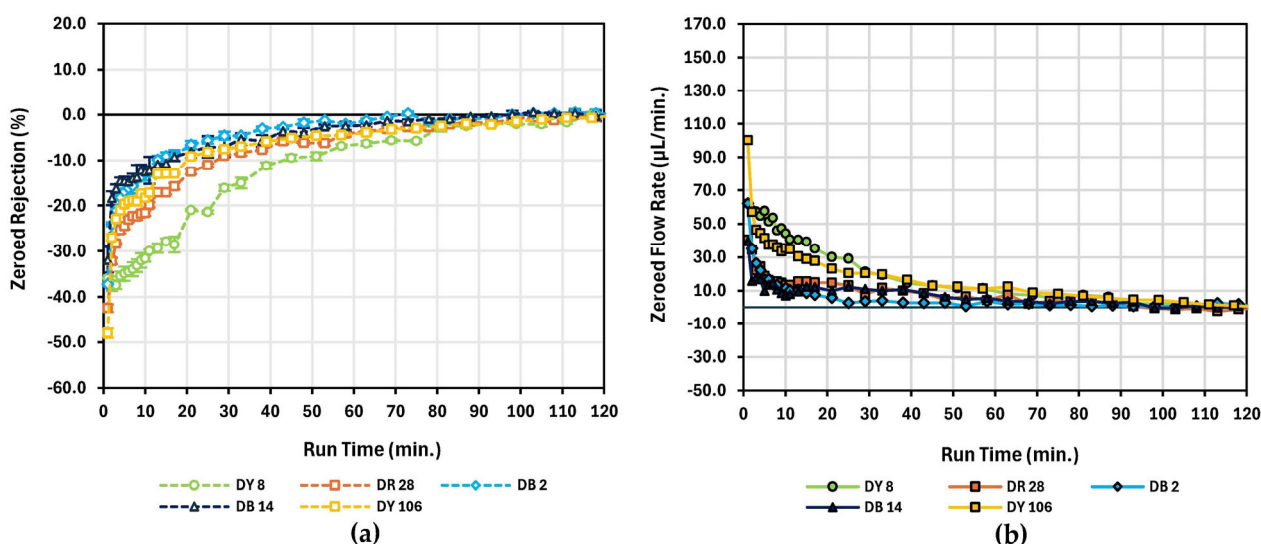


**Figure 6.** (a) Zeroed rejection as a function of time for the increasing intrinsic charge series at 1000 µM; (b) zeroed flow rate as a function of time for the increasing intrinsic charge series at 1000 µM. Closed data points represent flow rate values, and open data points represent rejection values. Light green circles—direct yellow 8 (DY 8), orange squares—direct red 28 (DR 28), light blue diamonds—direct blue 2 (DB 2), dark blue triangles—direct blue 14 (DB 14), and yellow squares—direct yellow 106 (DY 106).

If one abandons the confines that the dyes must be grouped into either (1) the negative two intrinsic charge data series or (2) the increasing intrinsic charge series from negative one to negative six and instead grouped based on the similarities in structure and functionality of the end groups, this may explain why direct red 28, direct blue 2, direct blue 14, and direct yellow 106 have similar rejection as a function of time plots in Figure 6a. As shown in Figure S1, these four dyes have double 6-carbon ring structures with sulphonates as their end groups (independent of intrinsic charge and other factors). This is a key observation in this research, leading to the realization that structure and functional end groups likely dominate over intrinsic charge when discussing trends in rejection data as a function of time. Let such dyes with double 6-carbon ring structures with sulphonate end groups belong to a data series called the symmetric sulphonates. Figure 7 illustrates the zeroed symmetric sulphonate series 2-h tests at 1000 µM for direct red 2, direct red 28, direct blue 2, direct blue 14, and direct yellow 106. Each test used separate unmodified polycarbonate filters. The rejection curves as a function of time share the same trends, indicating that these dyes possess similar performance characteristics for functionalizing the polycarbonate filters.

All other dyes tested that did not have double 6-carbon ring structures with sulphonates for both end groups or had different functional end groups entirely (independent of intrinsic charge) were grouped into a data set called the asymmetric functional end group series. As shown in Figure S1, only direct brown 2 and direct red 37 had one double 6-carbon ring structure as an end group with one and two sulphonates, respectively. Direct red 81 did have a double 6-carbon ring structure, but it was not located at the end of the molecule. The other dyes in this series, direct yellow 8 and direct yellow 12, had no double 6-carbon ring structures present in their molecules. The zeroed 2-h tests shown in Figure 8 for the asymmetric functional end group series at 1000 µM for direct yellow 8, direct red 81, direct red 37, direct yellow 12, and direct brown 2 did not possess an overall trend that aligned.

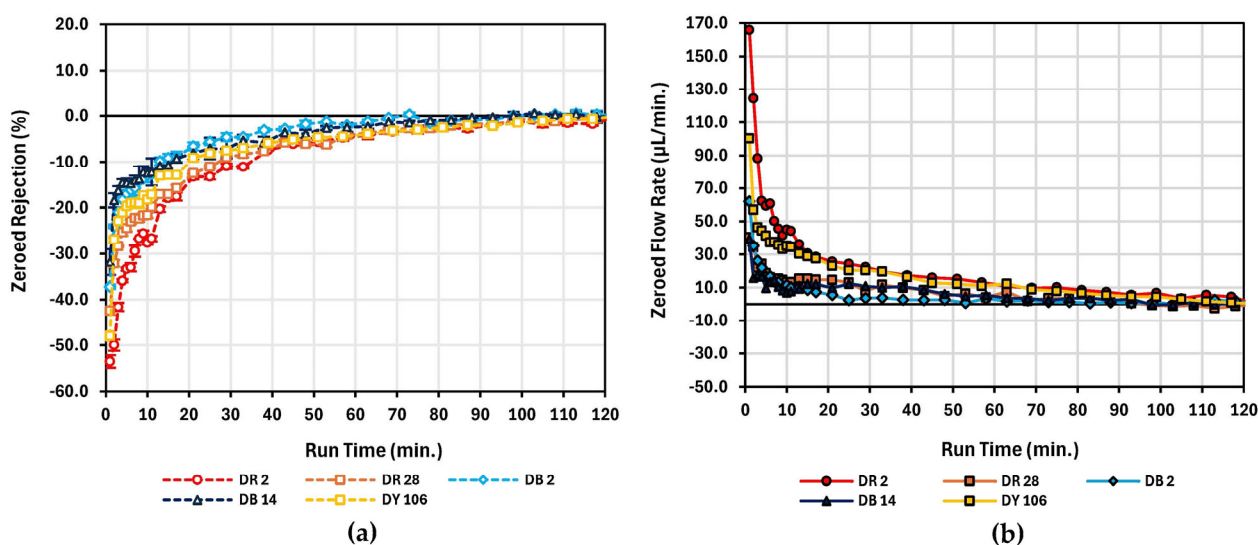


**Figure 7.** (a) Zeroed rejection as a function of time for the symmetric sulphonate series at 1000 µM; (b) zeroed flow rate as a function of time for the symmetric sulphonate series at 1000 µM. Closed data points represent flow rate values, and open data points represent rejection values. Red circles—direct red 2 (DR 2), orange squares—direct red 28 (DR 28), light blue diamonds—direct blue 2 (DB 2), dark blue triangles—direct blue 14 (DB 14), and yellow squares—direct yellow 106 (DY 106).

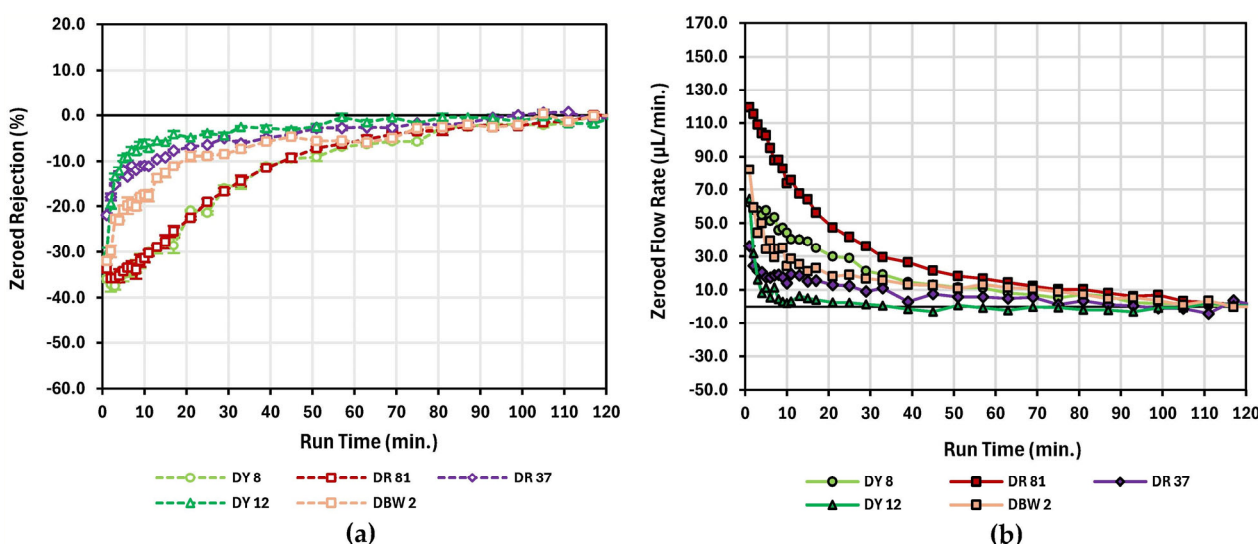
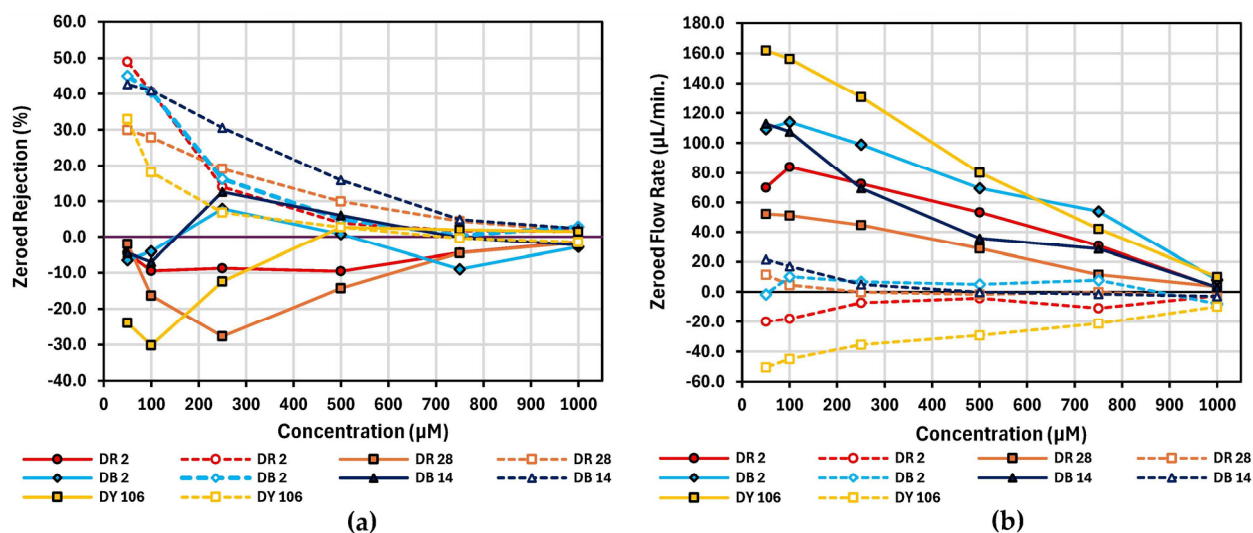


**Figure 8.** (a) Zeroed rejection as a function of time for the asymmetric functional end group series at 1000 µM; (b) zeroed flow rate as a function of time for the symmetric sulphonate series at 1000 µM. Closed data points represent flow rate values, and open data points represent rejection values. Light green circles—direct yellow 8 (DY 8), dark red squares—direct red 81 (DR 81), purple diamonds—direct red 37 (DR 37), green triangles—direct yellow 12 (DY 12), and light brown squares—direct brown 2 (DBW 2).

Having the dyes grouped based on similarities in structure, rejection as a function of increasing and decreasing concentration is examined next. Figure 9 illustrates the zeroed hysteresis tests for the symmetric sulphonate series (direct red 2, direct red 28, direct blue 2, direct blue 14, and direct yellow 106). The decreasing concentration tests do see an increase in rejection compared to the rejection present on the increasing concentration tests, demonstrating that functionalized polycarbonate membranes are effective at increasing the rejection of dyes at low concentrations post-functionalization, with functionalization effectively occurring at higher concentrations, as shown in previous research [32]. Any hysteresis in flow rate, or rejection, as concentration is decreased can be attributed to dyes



functionalizing the polycarbonate membrane. The flow rates of the decreasing concentration tests tend to be at a more constant rate, indicating the functionalizing is occurring with more prevalence at higher concentrations, not lower concentrations. The dyes in the symmetric sulphonate series, all of which have two double 6-carbon rings with sulphonates on their end groups, were able to functionalize an unmodified polycarbonate membrane, having an average hysteresis value of  $47.1 \pm 2.5\%$  at  $100 \mu\text{M}$ . At  $50 \mu\text{M}$  on the increasing concentration test, direct red 2 was pulled through the polycarbonate membrane 41 s longer than any other fluid; otherwise, all hysteresis tests were carried out as described in Section 2.5 with no major deviations. Any deviations, no matter how minor, from protocol are mentioned in the data files.



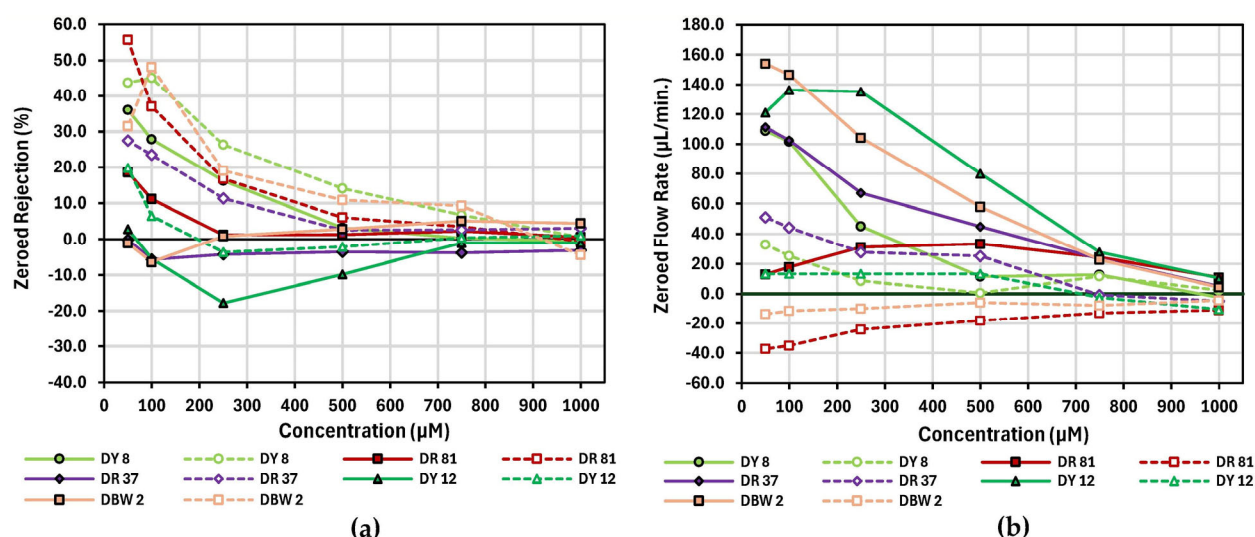
**Figure 9.** (a) Zeroed rejection as a function of concentration for the symmetric sulphonate series; (b) zeroed flow rate as a function of concentration for the symmetric sulphonate series. Solid data points connected by a solid line correspond to measurements made going from a low to high concentration, while open data points connected by a dashed line correspond to measurements made while going from a high to low concentration. Red circles—direct red 2 (DR 2), orange squares—direct red 28 (DR 28), light blue diamonds—direct blue 2 (DB 2), dark blue triangles—direct blue 14 (DB 14), and yellow squares—direct yellow 106 (DY 106).

Figure 10 illustrates the zeroed hysteresis tests for the asymmetric functional end group series (direct yellow 8, direct red 81, direct red 37, direct yellow 12, and direct brown 2). In many cases, the larger hysteresis values seen in the symmetric sulphonate series at  $100 \mu\text{M}$  are not present for these dyes in the asymmetric functional end group series, but as the data shows, they are still capable of functionalizing the porous polycarbonate membranes to some degree, typically leading to increases in rejection at low concentrations when decreasing in concentration post-functionalization. Any hysteresis as the concentration is decreased can be attributed to dyes functionalizing the polycarbonate membrane in some manner. The dyes in the asymmetric functional end group series, some of which have zero or only one double 6-carbon ring with sulphonates or other functional groups as their end groups, were able to functionalize an unmodified polycarbonate membrane, with an average hysteresis value of  $27.7 \pm 16.5\%$  at  $100 \mu\text{M}$ . This is a 41% decrease in the ability to functionalize the polycarbonate membranes compared to the symmetric sulphonate series.

For most dyes in Figures 9 and 10, the error bars (not shown in Figures 9 and 10 as to not distract from the average data, but present in the data file, and shown on each individual dye hysteresis graph) for flow rate are typically less than  $12 \mu\text{L}\cdot\text{min}^{-1}$  and less than 8% for rejection; however, this is not the case for direct red 81, direct brown 2, and direct blue 2 at concentrations of  $50 \mu\text{M}$ . These three dyes have considerable atypical



uncertainties in their rejection values at 50  $\mu\text{M}$ , ranging from 16.2% for direct red 81 to 33.5% for direct brown 2, which leads to uncertainties in the hysteresis differences at 50  $\mu\text{M}$ . The difference in hysteresis values is trusted at 100  $\mu\text{M}$ , where error bars in rejection do not exceed 8.0%, with most under 3.0%. The uncertainties at 50  $\mu\text{M}$  for the dyes are primarily related to the dyes starting to seemingly not reject from the surface of the polycarbonate filter, as observed for direct brown 2 and direct red 81 (in these cases, the permeate is nearly identical to the feed concentration for one out of the five experiments at each concentration). Similar observations were noted for direct blue 2 at 50  $\mu\text{M}$ .



**Figure 10.** (a) Zeroed rejection as a function of concentration for the asymmetric functional end group series; (b) zeroed flow rate as a function of concentration for the symmetric sulphonate series. Solid data points connected by a solid line correspond to measurements made going from a low to high concentration, while open data points connected by a dashed line correspond to measurements made while going from a high to low concentration. Light green circles—direct yellow 8 (DY 8), dark red squares—direct red 81 (DR 81), purple diamonds—direct red 37 (DR 37), green triangles—direct yellow 12 (DY 12), and light brown—direct brown 2 (DBW 2).

Table 2 provides dye characteristics such as absorbance wavelengths, intrinsic charge, information on the number of 6-carbon rings present, and hysteresis values for rejection measurements at 100  $\mu\text{M}$ , with the dyes grouped by the number of double 6-carbon rings in their chemical structure. Six of the dyes tested have an intrinsic charge of negative 2; however, the data in Table 2 illustrates that the intrinsic charge of the dyes is not the dominant variable that correlates with the hysteretic behavior observed at 100  $\mu\text{M}$ . The six dyes share similar intrinsic charges, have different structural characteristics, and have different dye rejection differences at 100  $\mu\text{M}$ . Direct red 2 (two double 6-carbon rings) and direct yellow 12 (zero double 6-carbon rings) are examples of this behavior, as both have the same intrinsic charge of negative 2, and both dyes illustrate a high variation in dye rejection differences at 100  $\mu\text{M}$  of 50.2% and 11.9%, respectively. Similarly, direct red 2 and direct yellow 106 have large differences in intrinsic charges of negative two and negative 6, respectively, but have only small differences in rejection hysteresis of 50.2% and 48.3% at 100  $\mu\text{M}$ , respectively.

Direct red 28, direct red 2, direct blue 2, direct blue 14, and direct yellow 106 have some of the largest recorded hysteresis values at 100  $\mu\text{M}$  after undergoing the functionalization process. These dyes have similar structural characteristics, such as sulphonate end groups with double 6-carbon rings, independent of intrinsic charge. The data summarized in Table 2 strongly suggests that structure plays a dominant role compared to intrinsic charge in this azo dye functionalization process of polycarbonate membranes. Overall, the data

illustrates dyes with zero, one, and two double 6-carbon ring structures are shown to have a systematic increase in their ability to functionalize the polycarbonate membranes, which is evident as changes in the 100  $\mu\text{M}$  dye solutions show increases in rejection pre- and post-functionalization of  $14.5\% \pm 3.7\%$ ,  $36.5\% \pm 15.7\%$ , and  $47.1\% \pm 2.5\%$ , respectively.

**Table 2.** Difference in average hysteresis rejection values for 100  $\mu\text{M}$  dye solutions grouped by number of double 6-carbon rings. Also provided is the absorbance wavelength used for each dye.

Dye Name	Intrinsic	Double	Single	Total	Diff. in Ave.			
	Charge (-)	6-Carbon Rings	6-Carbon Rings	6-Carbon Rings	$\lambda$ (nm)	100 $\mu\text{M}$ Hysteresis Rejection (%)	Ave (%)	Std (%)
Direct Red 2	2	2	2	6	535	50.2		
Direct Yellow 106	6	2	4	8	418	48.3		
Direct Blue 14	4	2	2	6	583	47.9		
Direct Blue 2	3	2	2	6	568	44.7		
Direct Red 28	2	2	2	6	490	44.2	47.1	2.5
Direct Brown 2	2	1	3	5	397	54.5		
Direct Red 81	2	1	3	5	511	25.9		
Direct Red 37	2	1	3	5	511	29.1	36.5	15.7
Direct Yellow 8	1	0	3	3	391	17.2		
Direct Yellow 12	2	0	4	4	406	11.9	14.5	3.7

As stated earlier, before and after each dye is tested, a minimum of 15 min of type 1 water is pulled through the polycarbonate membranes. This is performed to ensure the system is clean and not fouling pre-experiment and that the last 15 min of type 1 water wash at the end is not removing unbound dye molecules, demonstrating that the functionalization is permanent within the experimental setup. For the hysteresis tests involving direct red 81, direct red 28, and direct yellow 106, an additional 15 min of type 1 water was pulled through the filters between the 1000  $\mu\text{M}$  tests, with miniscule changes of less than  $5 \mu\text{L} \cdot \text{min}^{-1}$  in type 1 water flow rate for direct red 81 and direct red 28, meaning few unbound dye molecules were likely removed with this extra 15 min of type 1 water wash. Direct yellow 106 did see an average increase in the water flux of 22.7%. This increase in water flux for direct yellow 106 indicates some unbound dye molecules might have been removed during this additional wash cycle. If this additional wash cycle was not performed, the 100  $\mu\text{M}$  hysteresis difference would likely be slightly larger in magnitude, increasing the average hysteresis at 100  $\mu\text{M}$  for the symmetric sulphonate series. Based on Table 1, the large standard deviations for the post-wash cycle for direct blue 2, direct blue 14, and direct red 37 after hysteresis tests show they were the most unstable and would have likely benefitted from a longer washout cycle with type 1 water to see if a stable flow rate could be reached, providing more evidence that the functionalization is permanent for these three dyes under the given conditions.

#### 4. Conclusions

The results of this research demonstrate that azo dye pollutants that end up in wastewater streams may have the potential to be a sustainable part of the solution in the decolorization of the fresh water they pollute. In summary, the trends seen in the zeroed rejection and zeroed flow rate data as a function of both time and concentration align with trends seen in the structure and functional end group of dye molecules. While intrinsic charge might play an important role, it is not a dominant factor when determining a dye's capability to functionalize a polycarbonate membrane using this method. An increasing trend in the ability to functionalize the polycarbonate membranes at 100  $\mu\text{M}$  was observed for dyes with

an increasing number of double 6-carbon rings in their chemical structure, with increases in rejection pre- and post-functionalization ranging from  $14.5\% \pm 3.7\%$  to  $47.1\% \pm 2.5\%$ . Using this functionalization technique, where the azo dyes themselves are used as the functionalizing agents, 2 of the 10 dyes tested (direct blue 14 and direct red 28) were able to reject dye molecules at over 90% rejection at 50  $\mu\text{M}$ , with rejection hysteresis values between 44 and 48% at 100  $\mu\text{M}$ .

Direct brown 2 is the only dye in the study that possesses a carboxyl group. Direct brown 2 features one sulphonate end group and one carboxyl end group, which account for the negative two intrinsic charge of the dye molecule. During hysteresis testing, direct brown 2 featured unexplainable changes in its functionalization behavior, causing the dye to have a very high standard deviation for the data gathered during the decreasing concentration tests. This differing carboxyl end group may be an explanation for its behavior during hysteresis testing and for why it differs from the other dyes listed in Table 2. If direct brown 2 is excluded from the results in Table 2 due to its carboxyl end group, the systematically increasing trend in functionalization based on the number of double 6-carbon rings becomes even more pronounced. More analysis on dyes with carboxyl end groups would be necessary before reaching a proper conclusion on the effect that this specific end group has on azo dye polycarbonate membrane functionalization.

Some dyes, such as direct brown 2, visibly stain the filter, which could be due to the dye molecules chemically binding to the polycarbonate, leading to a reduced effective pore size; however, this would need to be confirmed via quantitative tests. The reduced flow rate observed could also be a result of the dye molecules interacting with each other in solution, resulting in them possessing a larger effective size. Or a combination of both could be occurring, leading to the observed results. If the dye molecules are binding to the surface, this could lead to an accumulated negative charge via a gel or cake layer, providing another pathway for the charged dye molecules to not only interact with other charged particles in solution but also provide them with a way to interact with a bound charge on the membrane [47].

With the world's access to freshwater resources limited and under the constant pressure of pollution, the long-term goal of this research is to understand how this sustainable functionalization process can be maximized to decolorize water. Many variables can be tested in the system in the future, such as pore radius of the polycarbonate filter to help determine if there is a critical pore size when this functionalization is dominant, porosity of the filter, different filter types, different dye types, systematically changing the pH in solution to test if aggregation of the dye molecules can be induced or controlled to enhance functionalization [48], systematically altering an additional salt concentration in the solution for the same purpose of testing if aggregation of the dye molecules can be induced or controlled to enhance functionalization [49], and changing the pressure at which dye is driven through the system, among others. The parameters of the dye molecules themselves, such as dye size, shape, and hydrophobicity, can also be investigated. Experiments that help quantify the amount of dye potentially bonded to the polycarbonate filter and those that contribute to molecular modeling would address the limitations of this work. Comparing these experimental values to available theories and/or models would be of great value for aiding in understanding the mechanisms at play at the functionalized filter's surface. Not having a quantitative measure of how the dye is interacting with the polycarbonate membrane is a major limitation of this work. Quantitative measurements of the mechanisms at play between the dye molecules and the polycarbonate surface would help to better define the word 'functionalization.' Future experiments beyond the initial single tests presented here would be of value to increase statistics for each dye tested. For practical applications, the evaluation of the long-term stability, reusability, regeneration,

and safety/toxicology implications of using such dye-functionalized membranes would need to be critically evaluated.

**Supplementary Materials:** The following supporting information can be downloaded at: <https://www.mdpi.com/article/10.3390/su17177696/s1>. Figure S1: The chemical structure for the negative 2 charge series; Figure S2: The chemical structure for the increasing charge series; Figure S3: Absorbance as a function of concentration for the 10 dyes used as functionalizing agents in this work; Figure S4: Comparing valid and failed tests with direct red 2 having different initial type 1 water flow rates; Figure S5: Comparing valid and failed tests with direct yellow 8 having different initial type 1 water flow rates; Table S1: A matrix of flow rate values obtained when comparing three different polycarbonate filters in three different stainless steel supporting screens at a vacuum pressure of 22 inHg (74.5 kPa); Figure S6: Raw rejection data compared to zero rejection data for direct red 28 at 1000  $\mu$ M; Figure S7: Raw direct red 28 flow rate data compared to zeroed flow rate data at 1000  $\mu$ M; Figure S8: Direct red 2 raw hysteresis flow rate data compared to zeroed hysteresis flow rate data. Additionally, discussions on (Section S.1) details of dye solution preparation, (Section S.2) initial type 1 water flow rates and sources of variation, and (Section S.3) zeroing hysteresis flow rate and 2-h test data can also be found here.

**Author Contributions:** Investigation, A.J.M., I.S.M., B.C., J.J. and S.P.M.; resources, S.P.M.; writing—original draft, A.J.M.; writing—review and editing, I.S.M., A.J.M., B.C., J.J. and S.P.M.; supervision, S.P.M.; project administration, S.P.M. All authors have contributed to revising the manuscript and contributed to the interpretation of data within it. All authors have read and agreed to the published version of the manuscript.

**Funding:** A.J.M. was supported in the summer of 2023 by the WV Higher Education Policy Commission, Science, Technology and Research Division under award SURE23-010 (Summer Undergraduate Research Experience program). In addition to financial support from Marshall University, A.J.M. would also like to thank the National Aeronautics and Space Administration (NASA) and West Virginia Space Grant Consortium for the 2023-2024 Undergraduate Research Fellowship program. This research was made possible by NASA West Virginia Space Grant Consortium, NASA Agreement# 80NSSC20M0055. I.S.M. acknowledges financial support through the National Science Foundation via the REU Site: Investigation of Subterranean Features in the Appalachian Region hosted at Marshall University (NSF Award #2149891), while B.C. and J.J. acknowledge financial support through the National Science Foundation via the REU Site: Appalachian Mathematics and Physics Site hosted at Marshall University (NSF Award #2349289). This material is based upon work supported by the National Science Foundation under Award No. (2349289 & 2149891). Any opinions, findings and conclusions or recommendations expressed in this material are those of the author(s) and do not necessarily reflect the views of the National Science Foundation. Finally, S.P.M. acknowledges the financial support and use of space from Marshall University needed to carry out this research.

**Institutional Review Board Statement:** Not applicable.

**Data Availability Statement:** All data presented in this study are openly available in the Marshall Digital Scholar repository. [https://mds.marshall.edu/physics\\_data/3/](https://mds.marshall.edu/physics_data/3/).

**Acknowledgments:** A special thanks to Michael Norton and those associated with the Molecular and Biological Imaging Center at Marshall University for use of the ND-1000 Spectrophotometer. No generative AI in any form was used in any aspect of this work.

**Conflicts of Interest:** The authors declare no conflicts of interest.

## References

1. Oki, T.; Kanae, S. Global Hydrological Cycles and World Water Resources. *Science* **2006**, *313*, 1068–1072. [[CrossRef](#)]
2. Oki, T.; Entekhabi, D.; Harrold, T.I. The Global Water Cycle. In *The State of the Planet: Frontiers and Challenges in Geophysics*; Sparks, R.S.J., Hawkesworth, C.J., Eds.; American Geophysical Union: Washington, DC, USA, 2004; Volume 150, pp. 225–337, ISBN 9780875904153. [[CrossRef](#)]

3. Shiklomanov, I.A. World Fresh Water Resources. In *World in Crisis: A Guide to the World's Fresh Water Resources*; Gleick, P.H., Ed.; Oxford University Press: New York, NY, USA, 1993; pp. 13–24.
4. Hosseiny, S.H.; Bozorg-Haddad, O.B.D. Water, Culture, Civilization, History. In *Economical, Political, and Social Issues in Water Resources*; Elsevier: Amsterdam, The Netherlands, 2021; pp. 189–216. [\[CrossRef\]](#)
5. Yevjevich, V. Water and Civilization. *Water Int.* **1992**, *17*, 163–171. [\[CrossRef\]](#)
6. Skorupta, A. The Development of Civilization. *Transformacje* **2023**, *4*, 590–611.
7. Population Today Home Page. Available online: <http://populationtoday.com> (accessed on 5 July 2025).
8. Gu, D.; Andreev, K.; Dupre, M.E. Major Trends in Population Growth Around the World. *China CDC Wkly.* **2021**, *3*, 604–613. [\[CrossRef\]](#)
9. Liu, J.; Yang, H.; Gosling, S.N.; Kumm, M.; Flörke, M.; Pfister, S.; Hanasaki, N.; Wada, Y.; Zhang, X.; Zheng, C.; et al. Water Scarcity Assessments in the Past, Present, and Future. *Earth's Future* **2017**, *5*, 545–559. [\[CrossRef\]](#)
10. Biyada, S.; Urbonavicius, J. Circularity in Textile Waste: Challenges and Pathways to Sustainability. *Clean Eng. Technol.* **2025**, *24*, 100905. [\[CrossRef\]](#)
11. Hunger, K. Dyes, General Survey. In *Industrial Dyes: Chemistry, Properties, Applications*; Hunger, K., Ed.; Wiley-VCH: Weinheim, Germany, 2003; pp. 1–12, ISBN 3-527-30426-6. [\[CrossRef\]](#)
12. Gičević, A.; Hindija, L.; Karačić, A. Toxicity of Azo Dyes in the Pharmaceutical Industry. In Proceedings of the International Conference on Medical and Biological Engineering, Banja Luka, Bosnia and Herzegovina, 16–18 May 2019; Volume 73, pp. 581–587. [\[CrossRef\]](#)
13. Bick, R.; Halsey, E.; Ekenga, C.C. The Global Environmental Justice of Fast Fashion. *Environ. Health* **2018**, *17*, 92. [\[CrossRef\]](#)
14. Tang, A.Y.L.; Lo, C.K.Y.; Kan, C.W. Textile Dyes and Human Health: A Systematic and Citation Network Analysis Review. *Color. Technol.* **2018**, *134*, 245–257. [\[CrossRef\]](#)
15. Islam, T.; Repon, M.; Islam, T.; Sarwar, Z.; Rahman, M. Impact of Textile Dyes on Health and Ecosystem: A Review of Structure, Causes, and Potential Solutions. *Environ. Sci. Pollut. Res.* **2023**, *30*, 9207–9242. [\[CrossRef\]](#)
16. Barbarossa, V.; Bosmans, J.; Wanders, N.; King, H.; Bierkens, M.F.P.; Huijbregts, M.F.P.; Schipper, A.M. Threats of Global Warming to the World's Freshwater Fishes. *Nat. Commun.* **2021**, *12*, 1701. [\[CrossRef\]](#)
17. Zhang, Y.; Liu, X.; Qi, B.; Shi, K.; Deng, J.; Zhou, Y. Aquatic Vegetation in Response to Increased Eutrophication and Degraded Light Climate in Eastern Lake Taihu: Implications for Lake Ecological Restoration. *Sci. Rep.* **2016**, *6*, 23867. [\[CrossRef\]](#)
18. Sharma, J.; Sharma, S.; Soni, V. Classification and Impact of Synthetic Textile Dyes on Aquatic Flora: A Review. *Reg. Stud. Mar. Sci.* **2021**, *45*, 101802. [\[CrossRef\]](#)
19. Scheffer, M. The Effect of Aquatic Vegetation on Turbidity; How Important are the Filter Feeders? *Hydrobiologia* **1999**, *408*, 307–316. [\[CrossRef\]](#)
20. Pant, K.; Palanisamy, P. Navigating the Path to Industry 4.0: A Study on Key Barriers in Indian Textile Supply Chain. *Benchmarking Int. J.* **2025**. ahead-of-print. [\[CrossRef\]](#)
21. Mustafa, S.; Mahmood, F.; Shafqat, U.; Hussain, S.; Shahid, M.; Batool, F.; Elnour, R.; Hashem, M.; Asseri, T.; Shahzad, T. The Biosynthesis of Nickel Oxide Nanoparticles: An Eco-Friendly Approach for Azo Dye Decolorization and Industrial Wastewater Treatment. *Sustainability* **2023**, *15*, 14965. [\[CrossRef\]](#)
22. Samy, M.; Elkady, M.; Kamal, A.; Eleessawy, N.; Zaki, S.; Eltarahony, M. Novel Biosynthesis of Graphene-Supported Zero-Valent Iron Nanohybrid for Efficient Decolorization of Acid and Basic Dyes. *Sustainability* **2022**, *14*, 14188. [\[CrossRef\]](#)
23. Abbas, S.H.; Kamar, F.H.; Al-Saadi, S.; Albayati, T.M. Decolorization of Azo Dye from Synthetic Wastewater using the Fenton Oxidation Process. *Earth Environ. Sci.* **2025**, *1507*, 012035. [\[CrossRef\]](#)
24. Strebel, A.; Behringer, M.; Hilbig, H.; Machner, A.; Helmreich, B. Anionic Azo Dyes and their removal from Textile Wastewater through Adsorption by Various Adsorbents: A Critical Review. *Front. Environ. Eng.* **2024**, *3*, 1347981. [\[CrossRef\]](#)
25. Benkhaya, S.; Lgaz, H.; Alrashdi, A.; M'rabet, S.; El Bachiri, A.; Assouag, M.; Chung, I.; El Harfi, A. Upgrading the Performances of Polysulfone/Polyetherimide Ultrafiltration Composite Membranes for Dye Removal: Experimental and Molecular Dynamics Studies. *J. Mol. Liq.* **2021**, *331*, 115743. [\[CrossRef\]](#)
26. Benkhaya, S.; M'rabet, S.; Hsissou, R.; El Harfi, A. Synthesis of New Low-Cost Organic Ultrafiltration Membrane Made from Polysulfone/Polyetherimide Blends and its Application for Soluble Azoic Dyes Removal. *J. Mater. Res. Technol.* **2020**, *9*, 4763–4772. [\[CrossRef\]](#)
27. El-Sheekh, M.M.; Shafay, S.M.E.; El-Shanshoury, A.E.R.; Hamouda, H.; Gharieba, D.Y.; Abou-El-Souod, G.W. Impact of Immobilized Algae and its Consortium in Biodegradation of the Textile Dyes. *Int. J. Phytoremediat.* **2023**, *25*, 687–696. [\[CrossRef\]](#)
28. Adesanmi, B.M.; Hung, Y.T.; Paul, H.; Huhnke, C. Comparison of Dye Wastewater Treatment Methods: A Review. *GSC Adv. Res. Rev.* **2022**, *10*, 126. [\[CrossRef\]](#)
29. Benkhaya, S.; M'rabet, S.; El Harf, A. Classifications, Properties, Recent Synthesis and Applications of Azo Dyes. *Heliyon* **2020**, *6*, e03271. [\[CrossRef\]](#)



30. Stolz, A. Basic and Applied Aspects in the Microbial Degradation of Azo Dyes. *Appl. Microbiol. Biotechnol.* **2001**, *56*, 69–80. [CrossRef]
31. Aspland, J. Direct Dyes and their Application. *Text. Chem. Color.* **1991**, *23*, 41–45.
32. Cockerham, C.; Caruthers, A.; McCloud, J.; Fortner, L.; Youn, S.; McBride, S. Azo-Dye-Functionalized Polycarbonate Membranes for Textile Dye and Nitrate Ion Removal. *Micromachines* **2022**, *13*, 577. [CrossRef] [PubMed]
33. Christie, R.M. *Colour Chemistry*, 2nd ed.; The Royal Society of Chemistry: Cambridge, UK, 2015; ISBN 978-1-84973-328-1.
34. Chequer, F.M.; Dorta, D.J.; de Oliveira, D.P. Azo Dyes and their Metabolites: Does the Discharge of the Azo Dye into Water Bodies Represent Human and Ecological Risks? In *Advances in Treating Textile Effluent*; Hauser, P., Ed.; IntechOpen: London, UK, 2011; ISBN 978-953-307-704-8.
35. Rápó, E.; Tonk, S. Factors Affecting Synthetic Dye Adsorption; Desorption Studies: A Review of Results from the Last Five Years (2017–2021). *Molecules* **2021**, *26*, 5419. [CrossRef] [PubMed]
36. National Center for Biotechnology Information. PubChem 2D Structure Image of CID 11313, Congo Red. Available online: <https://pubchem.ncbi.nlm.nih.gov/compound/11313#section=2D-Structure> (accessed on 25 June 2025).
37. National Center for Biotechnology Information. PubChem 2D Structure Image of CID 17462, Solaminrot 4B. Available online: <https://pubchem.ncbi.nlm.nih.gov/compound/17462#section=2D-Structure> (accessed on 25 June 2025).
38. National Center for Biotechnology Information. PubChem 2D Structure Image of CID 17067, Direct Brown 2. Available online: <https://pubchem.ncbi.nlm.nih.gov/compound/17067#section=2D-Structure> (accessed on 25 June 2025).
39. National Center for Biotechnology Information. PubChem 2D Structure Image of CID 13816, C.I. Direct Red 2. Available online: <https://pubchem.ncbi.nlm.nih.gov/compound/13816#section=2D-Structure> (accessed on 25 June 2025).
40. National Center for Biotechnology Information. PubChem 2D Structure Image of CID 165134, 1,3-Naphthalenedisulfonic Acid, 8-(2-(4'-(2-(4-Ethoxyphenyl)diazenyl)(1,1'-biphenyl)-4-yl)diazenyl)-7-hydroxy-, Sodium Salt (1:2). Available online: <https://pubchem.ncbi.nlm.nih.gov/compound/165134#section=2D-Structure> (accessed on 25 June 2025).
41. National Center for Biotechnology Information. PubChem 2D Structure Image of CID 6364584, Direct Yellow 12. Available online: <https://pubchem.ncbi.nlm.nih.gov/compound/6364584#section=2D-Structure> (accessed on 25 June 2025).
42. National Center for Biotechnology Information. PubChem 2D Structure Image of CID 135848150, 7-Benzothiazolesulfonic Acid, 6-Methyl-2-(4-((2-oxo-1-((phenylamino)carbonyl)propyl)azo)phenyl)-, Monosodium Salt. Available online: <https://pubchem.ncbi.nlm.nih.gov/compound/135848150#section=2D-Structure> (accessed on 25 June 2025).
43. National Center for Biotechnology Information. PubChem 2D Structure Image of CID 17057, C.I. Direct Blue 2. Available online: <https://pubchem.ncbi.nlm.nih.gov/compound/17057#section=2D-Structure> (accessed on 25 June 2025).
44. National Center for Biotechnology Information. PubChem 2D Structure Image of CID 6296, Trypan Blue. Available online: <https://pubchem.ncbi.nlm.nih.gov/compound/6296#section=2D-Structure> (accessed on 25 June 2025).
45. National Center for Biotechnology Information. PubChem 2D Structure Image of CID 6538333, C.I. Direct Yellow 106. Available online: <https://pubchem.ncbi.nlm.nih.gov/compound/6538333#section=2D-Structure> (accessed on 25 June 2025).
46. Cole, K.; Levine, B.S. Ultra Visible Spectrophotometry. In *Principles of Forensic Toxicology*, 5th ed.; Levine, B.S., Kerrigan, S., Eds.; Springer: Berlin/Heidelberg, Germany, 2020; pp. 127–134, ISBN 978-3030429164.
47. Cirillo, A.; Tomaiuolo, G.; Guido, S. Membrane Fouling Phenomena in Microfluidic Systems: From Technical Challenges to Scientific Opportunities. *Micromachines* **2021**, *12*, 820. [CrossRef]
48. Ahmad, A.; Harris, W. Removal of Dye from Wastewater of Textile Industry using Membrane Technology. *J. Teknol.* **2022**, *26*, 31–44. [CrossRef]
49. Mooi, S.; Heyne, B. Size does Matter: How to Control Organization of Organic Dyes in Aqueous Environment using Specific Ion Effects. *Langmuir* **2012**, *28*, 16524–16530. [CrossRef]

**Disclaimer/Publisher's Note:** The statements, opinions and data contained in all publications are solely those of the individual author(s) and contributor(s) and not of MDPI and/or the editor(s). MDPI and/or the editor(s) disclaim responsibility for any injury to people or property resulting from any ideas, methods, instructions or products referred to in the content.